Wu et al. Nanoscale Research Letters (2018) 13:144
https://doi.org/10.1186/s11671-018-2564-8

Nanoscale Research Letters

NANO EXPRESS Open Access

Optically Active Plasmonic Metasurfaces based on the Hybridization of In-Plane Coupling and Out-of-Plane Coupling

Dong Wu[1†], Liu Yang[1†], Chang Liu[1], Zenghui Xu[1], Yumin Liu[1*], Zhongyuan Yu[1], Li Yu[1,2], Lei Chen[1], Rui Ma[1] and Han Ye[1]

Abstract

Plasmonic metasurfaces have attracted much attention in recent years owing to many promising prospects of applications such as polarization switching, local electric field enhancement (FE), near-perfect absorption, sensing, slow-light devices, and nanoantennas. However, many problems in these applications, like only gigahertz switching speeds of electro-optical switches, low-quality factor (Q) of plasmonic resonances, and relatively low figure of merit (FOM) of sensing, severely limit the further development of plasmonic metasurface. Besides, working as nanoantennas, it is also challenging to realize both local electric FE exceeding 100 and near-perfect absorption above 99%. Here, using finite element method and finite difference time domain methods respectively, we firstly report a novel optically tunable plasmonic metasurface based on the hybridization of in-plane near-field coupling and out-of-plane near-field coupling, which provides a good solution to these serious and urgent problems. A physical phenomenon of electromagnetically induced transparency is obtained by the destructive interference between two plasmon modes. At the same time, ultrasharp perfect absorption peaks with ultra-high Q-factor (221.43) is achieved around 1550 nm, which can lead to an ultra-high FOM (214.29) in sensing application. Particularly, by using indium-doped CdO, this metasurface is also firstly demonstrated to be a femtosecond optical reflective polarizer in near-infrared region, possessing an ultra-high polarization extinction ratio. Meanwhile, operating as nanoantennas, this metasurface achieves simultaneously strong local electric FE($|E_{loc}|/|E_0| > 100$) and a near-perfect absorption above 99.9% for the first time, which will benefit a wide range of applications including photocatalytic water splitting and surface-enhanced infrared absorption.

Keywords: Plasmonics, Metamaterials, Optical switching devices, Optical sensing and sensors, Subwavelength structures, Nanostructures

Background

Plasmonic metasurfaces, as two-dimensional versions of metamaterials, have a wide range of promising phenomena and applications including polarization switching [1], beam rotator [2], Fano resonance [3–7], nanoantennas [8–10], negative refractive index [11, 12], near-perfect absorbers [13–15], and invisibility cloaking. Especially, much attention has been paid to studying of electromagnetically induced transparency (EIT) phenomenon and Fano resonance based on plasmonic metasurfaces owing to many potential applications such as surface-enhanced Raman scattering (SERS) [3], surface-enhanced infrared absorption (SEIRA) [16], refractive index sensing [17–21], and quantum information storages. The concepts of EIT and Fano resonance both are originally discovered in quantum system. EIT is obtained by the destructive interference between two plasmon modes in classic system. Then, if the EIT is generated when a narrower plasmon mode destructively interferes with a broader plasmon mode, the resulting spectrum will have a Fano line shape. Zhang et al. firstly realized Fano resonance and EIT in a plasmonic nanostructure with a bright and dark element in one plane

* Correspondence: microliuyumin@hotmail.com
Dong Wu and Liu Yang contributed equally to this work.
†Equal contributors
[1]State Key Laboratory of Information Photonics and Optical Communications, Beijing University of Posts and Telecommunications, Beijing 100876, China
Full list of author information is available at the end of the article

[22]. However, for most of reported plasmonic metasurfaces based on in-plane plasmonic coupling operating in a visible or near infrared (NIR) region, the coupling strength is determined by the accurate size of gap between resonant elements, but achieving precise, sub-10-nm gaps still is a challenge due to the limitations of current fabrication technology [8]. But these nanostructures strongly rely on the tiny inter-particle distance, which is not favorable to the large-area production. Different from the metasurface based on in-plane coupling effect, Liu et al. experimentally demonstrated plasmonic EIT using vertical stacking of the metamaterial elements for the first time [23]. Subsequently, a number of metamaterials (or metasurfaces) based on the planar or vertical design of plasmonic nanostructures are recently proposed and demonstrated to achieve EIT-like phenomena and Fano resonances [24–35]. Amin et al. demonstrated the asymmetric Fano-like spectral line-shape and a narrow EIT window in the response of the resonator constructed using both the gold frame and the graphene patch in one plane [17]. However, the quality factor of the Fano resonance in this metal structure is very low owing to optical losses in metal that cause significant broadening of the plasmonic resonances, which also is an extremely common problem in plasmonic nanostructures using metals [36–42]. To our knowledge, the Q-factors of most reported Fano resonances at visible and NIR region are generally lower than 10 [36–43]. Recently, Dayal et al. demonstrated a whispering-gallery-mode-based metallic metasurfaces realizing high Q (reaching 79) plasmonic Fano resonances at NIR frequencies [5]. However, this reported Fano resonance can only be achieved at a specific wavelength, which also is another common problem seriously restricting the further developments and applications of the Fano resonance or EIT phenomena. The active manipulation of Fano resonance or EIT window is highly desirable for many practical applications [19, 21, 35, 43]. Xia et al. designed and numerically demonstrated a tunable PIT system composed of sinusoidally curved and planar graphene layers, which can avoid any of the patterns of the graphene sheet [44]. In 2017, Yang et al. experimentally achieved a highly controllable absorption resonance with high-quality factor, which are firstly demonstrated to be a femtosecond optical polarization switching based on a plasmonic metasurface in a mid-infrared region [1]. Besides, a maximum electric field enhancement reaching 41.8 is also observed in this work. It is desirable to employ plasmonic nanoantennas that result in not only "hot spots" with a large local field enhancement but also a near-perfect absorption. Although tremendous progress in the exploration of enhancing the local electric field enhancement and improving the absorption, achieving strong local electric field enhancements ($|E_{loc}|/|E_0| > 100$) and near-perfect absorption (> 99%) simultaneously still remains a challenge, which will benefit a wide range of applications including plasmonic sensors, photocatalytic water splitting, SERS, and SEIRA. On the other hand, except for the polarization switching reported by Yang et al. [1], most traditional polarization-selective devices, such as waveplates and polarizers based on electro-optical effects, are either static or operating with only gigahertz switching speeds, which are limited by the required electronics [45, 46]. Thus, for the phenomena or applications of EIT effect, Fano resonance, and plasmonic nanoantennas based on a plasmonic metasurface, most of previously reported works usually suffer from these serious and urgent problems: (i) the broadening of plasmonic resonances owing to large optical losses in metals [5]; (ii) unadjustable operating wavelength of EIT effect or Fano resonances [35]; (iii) the challenge of achieving strong local electric field enhancements ($|E_{loc}|/|E_0| > 100$) and near-perfect absorption (> 99%) simultaneously [8]; (iv) generally, only gigahertz switching speeds of polarization-selective devices operating in visible or NIR region [1].

In this work, using finite difference time domain (FDTD) and finite element method (FEM) respectively, we propose and numerically demonstrate an optically active plasmonic metasurface based on the hybridization of in-plane coupling and out-of-plane coupling. In this metasurface system, the EIT-like effect can be achieved by breaking the structure symmetry, and the operating wavelength of the EIT widows can be tuned by changing the refractive index of the CdO layer, which can be optically controlled by tuning the pump light [1]. In this EIT-like reflection spectrum, a high Q-factor plasmonic resonance is obtained at a wavelength of 1550 nm, which is much higher than that of previously reported works [36–43]. Particularly, owing to the polarization independence of the metasurface, this plasmonic metasurface using In-doped cadmium also can function as a femtosecond polarization switch for TM-polarized light at 1550 nm. By tuning the pump light, we spectrally redshift the plasmonic resonances, and the metasurface achieves a large modulation depth of the reflection of the TM-polarized light from 0.003 to 60%, while maintaining a near-one reflection for the TE-polarized wave. To our knowledge, such a large modulation depth is far higher than those of previously reported plasmonic switch systems [47–55]. Note that the femtosecond polarization switch is firstly numerically demonstrated based on the plasmonic metasurface via the hybridization of in-plane coupling and out-of-plane coupling. At the same time, this metasurface can achieve near-perfect absorption above 99.9% and maximum electric field enhancement reaching 108 simultaneously, and the strong electric enhancement is confined within a circular area with a diameter of only 3 nm, which is very beneficial to single molecule detection for many surface-enhanced spectroscopies. Besides, owing to the sensitivity of

refractive index changing and the ultra-sharp plasmonic resonance, this metasurface also can work as an ultra-high figure of merit (FOM) refractive index sensor.

Methods

The proposed metasurface is schematically shown in Fig. 1a. Figure 1b presents the cross section of one unit cell of the metasurface with geometric parameters, which consists of two groups of gold bars and a polymer layer. Each group has two gold bars separated by a nanoslit. One group of gold bars is placed on the polymer layer, and the other group of gold bars was embedded in the polymer layer. The asymmetric gold nanobar array is periodically arranged on the thick gold substrate with a periodicity of $P = 1395$ nm. The proposed metasurface is illuminated by a normally incident transverse-magnetic (TM) light (the magnetic component perpendicular to the incident light). In this calculation, to ensure the reliability and accuracy of the simulated results, we employ FDTD and FEM methods to calculate the optical properties and electromagnetic field distributions of the proposed metasurface, respectively. The FEM calculation is performed by commercial software COMSOL MULTIPHYSICS. The period boundary condition is applied in the x direction and we set the perfectly matched layer (PML) on the boundary of the y direction. The mesh size is 0.8 nm in both x and y directions. The permittivity of Au is described by the Drude model, and the refractive index of the polymer is 1.5 [36, 56, 57]. The simulation background is assumed in air with $n_{air} = 1$. The absorption is given by $A = 1 - R$, owing to an opaque Au substrate ($T = 0$) [58].

Results and Discussion

As shown in Fig. 2a, we calculate and depict the reflection and absorption spectra of the proposed metasurface around 1550 nm at normal incidence under TM-polarized light. For the absorption spectrum, there are two distinct absorption peaks located at 1550 and 1588 nm with a near-perfect absorption efficiency above 99.9%, respectively. From the reflection spectrum shown in Fig. 2b, we observe an EIT-like spectral response of this metasurface in this wavelength range, and the same results of reflection spectra are demonstrated by using FDTD and FEM, respectively. The reflection spectrum of the proposed metasurface under TE polarization (the electric component perpendicular to the incident plane) is also presented in Fig. 2b with a black line, and the reflection is close to one indicating no absorption occurs in this metasurface for TE polarization. The polarization dependence of this metasurface can be easily explained by the asymmetric design of the proposed metasurface. Therefore, this metasurface couples efficiently for TM polarization and remains dark for TE polarization.

To easily explain the EIT-like phenomenon of the proposed metasurface in Fig. 2a, we initially consider a relatively simple metasurface without nanoslit shown in Fig. 2c, which is composed of two gold nanobars with different distances from gold substrate. The reflection spectrum of this metasurface without nanoslit is calculated and depicted in Fig. 2d. Clearly, an EIT-like spectral response with an asymmetric line shape emerges, which may be due to the coupling effect between the two gold bars. Then, the symmetry-breaking process (Fig. 3a-c) of the structure is investigated to clarify underlying forming process of the EIT-like window. The variations of the reflective spectra with changing Δd are calculated and depicted in Fig. 3d. For $\Delta d = 0$, there is only one reflection dip around 1653 nm in the working waveband, as shown in Fig. 3e. As Δd increases, we notice that there appear the EIT-like spectral response with two reflection dips (ω_{Left} and ω_{Right}). If further increasing Δd, the ω_{Left} mode can be further enhanced, and these calculated results indicate that the ω_{Left} mode may be very relevant to the gold nanobar A. At the same time, with increasing Δd, the resonance wavelength of ω_{Left} mode show slight red shift, and the resonance wavelength of ω_{Right} mode remains almost no change around 1653 nm. Through the above analysis, the generation of EIT-like phenomena can be contributed to the asymmetry of the nanostructure. Besides, to interpret the plasmonic resonance at 1395 nm in the reflection spectra shown in Fig. 3d, g, the reflection spectra are compared between the designed metasurface and metallic grating structure (see insert of Fig. 3g). For the metallic grating structure, there is also a resonance dip at 1395 nm, resulting from the excitation of surface

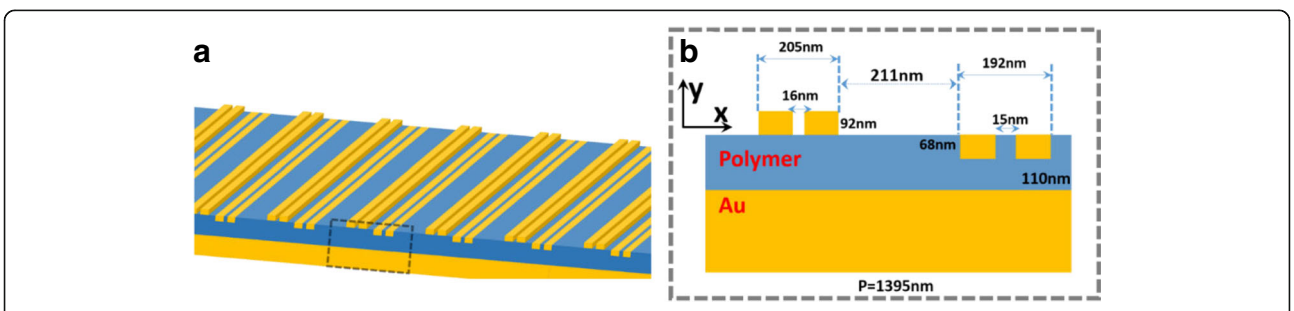

Fig. 1 **a** Schematic structure of the proposed metasurface. **b** Cross section of the plasmonic metasurface with the geometric parameters

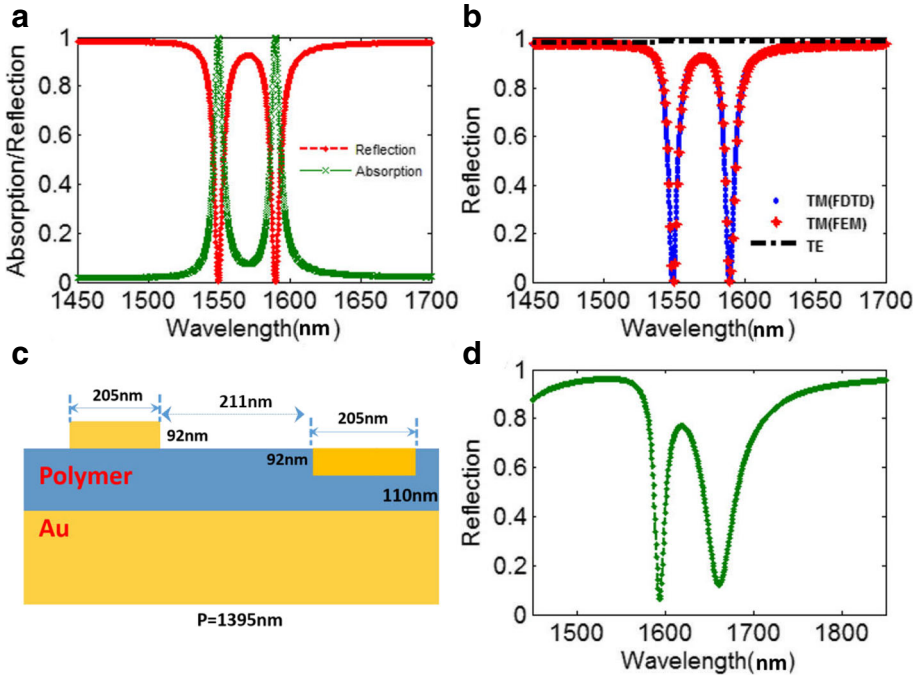

Fig. 2 **a** Absorption and reflection spectra of the plasmonic metasurface shown in Fig. 1. **b** The reflection spectra of the metasurface shown in Fig. 1 calculated by FDTD and FEM, respectively. **c** The plasmonic metasurface composed of two gold bars with different distances from gold substrate. **d** Reflection spectrum of the plasmonic metasurface shown in **c**

plasmon polariton (SPP) from previously reported studies [58, 59]. Thus, the plasmonic resonance of this metasurface at 1395 nm is caused by the excitation of SPP.

Then, we also respectively investigate the reflection spectra of the metasurface constructed using film-coupled nanobar systems with only the gold nanobar A and the gold nanobar B, as shown in Fig. 4a, b. When excited with TM incident light separately, a narrower plasmon mode (ω_A) is excited in the metasurface with gold nanobar A, and a broader plasmon mode (ω_B) is observed in the metasurface with gold nanobar B. To more clearly illustrate the physical mechanism behind these two plasmon modes, we respectively calculate the magnetic field distributions at these two reflection dips, as shown in Fig. 4c, d. The red arrows present currents whereas the color map presents the magnitude of the magnetic field. For the ω_A mode shown in Fig. 4a, it can be observed that the magnetic field is confined to the gap between the gold nanobar A and the gold substrate. Besides, the antiparallel currents are observed at top and bottom internal metallic interfaces. Therefore, the plasmon mode is primarily associated with magnetic resonance caused by circulating currents, and the incident light energy is dissipated by the ohmic loss of metal, causing the reflection dip in ω_A mode. Then, for the ω_B mode in Fig. 4b, the circulating currents are in the opposite direction to that of the currents of the ω_A mode, which also can excite the magnetic resonance. For the film-coupled nanobar system with both gold nanobar A and the gold nanobar B, the phenomenon in Fig. 5a also can be treated as double Fano resonances with two reflection dips (ω_{Left} and ω_{Right}) owing to the asymmetric line shape [3]. This asymmetric Fano-like spectral line shape and an EIT-like window is obtained from the destructive interference between the narrower plasmon mode (ω_A) shown in Fig. 4a and the broader plasmon mode (ω_B) shown in Fig. 4b. To our knowledge, Fano resonances are first observed in artificially structured arrays of same shaped resonators with asymmetrical positions.

To further explore the physical mechanism behind these two plasmonic resonances (ω_{Left} and ω_{Right}) shown in Fig. 4c, the magnetic field H and electric field $|E_{loc}|/|E_0|$ distributions at the wavelengths of these two resonances are calculated and depicted in Fig. 5. On the one hand, according to Fig. 5b, c, the magnetic fields are mainly localized at the dielectric layer between the gold nanobars and the gold substrate, which is the key feature of the out-of-plane coupling between the gold bars and the Au substrate. Clearly, different field distributions are observed for these two resonances excited at two absorption peaks. For the ω_{Left} mode, the magnetic field is localized at the gap between the gold nanobar A and the gold substrate, indicating that the ω_{Left} mode is closely related to the out-of-plane coupling between the gold nanobar A and the gold substrate, which is similar but not the same as the magnetic field of the ω_A mode in Fig. 4c owing to the coupling between the ω_A mode and ω_B mode. For theω_{Right} mode, the magnetic field is localized at the

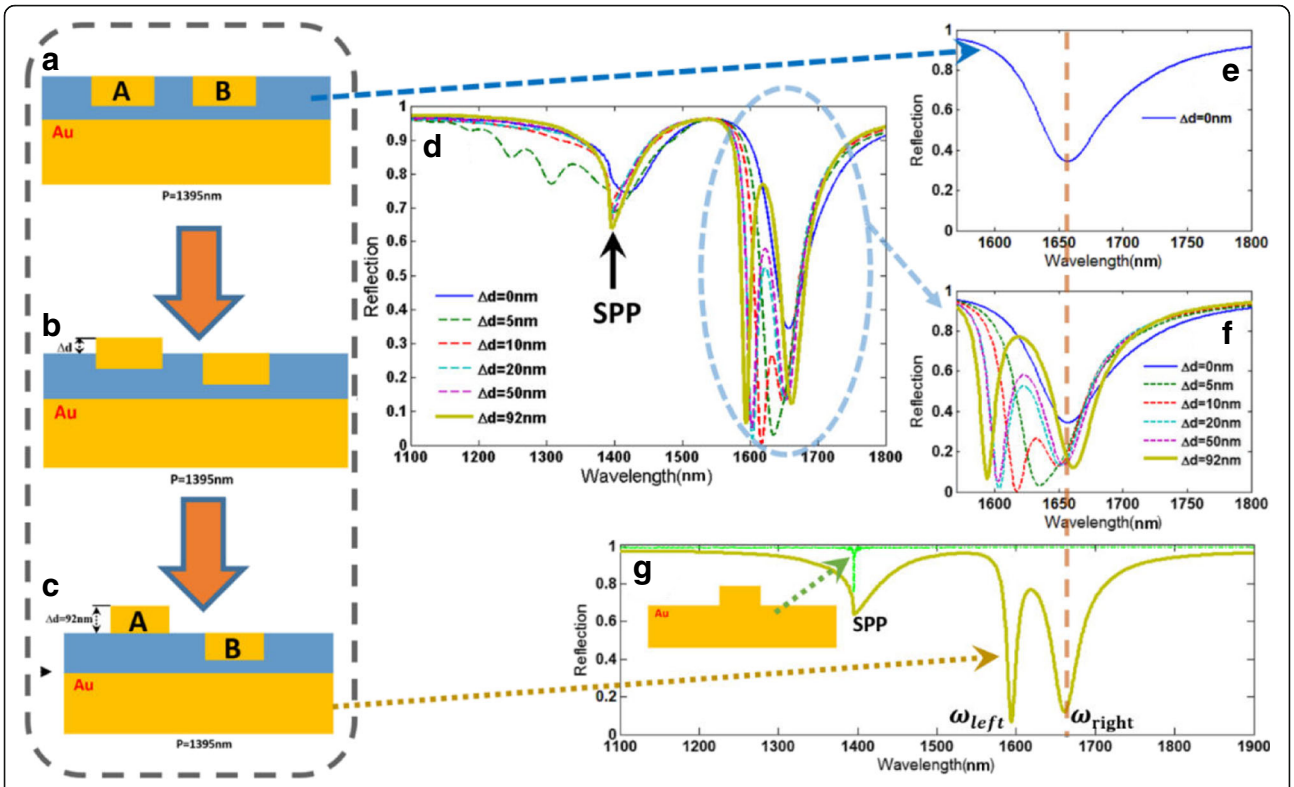

Fig. 3 **a**–**c** The symmetry-breaking process of the plasmonic metasurface shown in Fig. 2c. **d** The reflection spectra of the plasmonic metasurface with various Δd at the wavelength range of 1100–1800 nm. **e** The reflection spectrum of the plasmonic metasurface with $\Delta d = 0$ at the wavelength range of 1550–1800 nm. **f** The reflection spectra of the plasmonic metasurface with various Δd at the wavelength range of 1550–1800 nm. **g** The reflection spectra of the plasmonic metasurface with various $\Delta d = 92$ nm and the all metal structure at the wavelength range of 1100–1800 nm, respectively

nanogap between the gold nanobar B and the substrate. Therefore, the ω_{Right} mode is mainly contributed to the out-of-plane coupling between the gold nanobar B and the gold substrate. On the other hand, the electric fields are strongly enhanced and localized in an ultrasmall area at the edges of the gold bars. Then, except for the physical phenomena of EIT, this metasurface also can be treated as plasmonic nanoantennas (PNs), confining the free-space incident lights into sub-wavelength region with the local field enhancement, which is a very important and fundamental research for nanophotonic systems. Here, the factor $|E_{\mathrm{loc}}|/|E_0|$ is defined to evaluate the performance of local electric field enhancements of PNs. As shown in Fig. 5d, e, the local electric field enhancements of the metasurface can reach as high as 75. However, although local electric field enhancements are achieved using film-coupled nanobar systems, according to Fig. 4c, there is still a considerable amount of work to be done to realize a near-perfect absorption, which results in a small modulation depth. From previous researches [8], we know that achieving both large local electric field enhancement and near-perfect absorption will benefit a wide range of applications, including plasmonic sensors, photocatalytic water splitting, SERS, and SEIRA. Besides, this metasurface structure shows a relatively broader linewidth. Because the Q-factor of plasmonic resonance is defined as $Q = \lambda/\text{full width at half maximum (FWHM)}$, a broader resonance will lead to a lower Q plasmonic resonance. Therefore, the broad FWHM and small modulation depth of those resonances may hamper applications such as refractive index sensing, polarization switching, and slowing down light, where a sharp spectral response is desired.

To simultaneously realize large local electric field enhancement, near-perfect absorption, and high Q-factor resonance, here we introduce the concept of the hybridization of out-of-plane plasmon coupling and in-plane plasmon coupling in this work. Clearly, compared with the film coupled nanobar metasurface based on out-of-plane coupling, this proposed metasurface in Fig. 1 has superior absorption properties as shown in Fig. 2. Particularly, the FWHM of the plasmonic resonance at 1550 nm is 7 nm, resulting in a Q-factor ($Q = \lambda/\mathrm{FWHM} = 1550\ \mathrm{nm}/7\ \mathrm{nm}$) of 221.43, which is much higher than those of previously reported works [36–42]. Then, in order to gain further physical insights into the high-Q Fano resonances and the perfect absorption arising from the original metasurface in Fig. 1, we plot the simulated magnetic and electric field distribution at resonance wavelengths of 1550 nm (ω_1) and 1588 nm (ω_2), as shown in Fig. 6. Clearly, the magnetic field

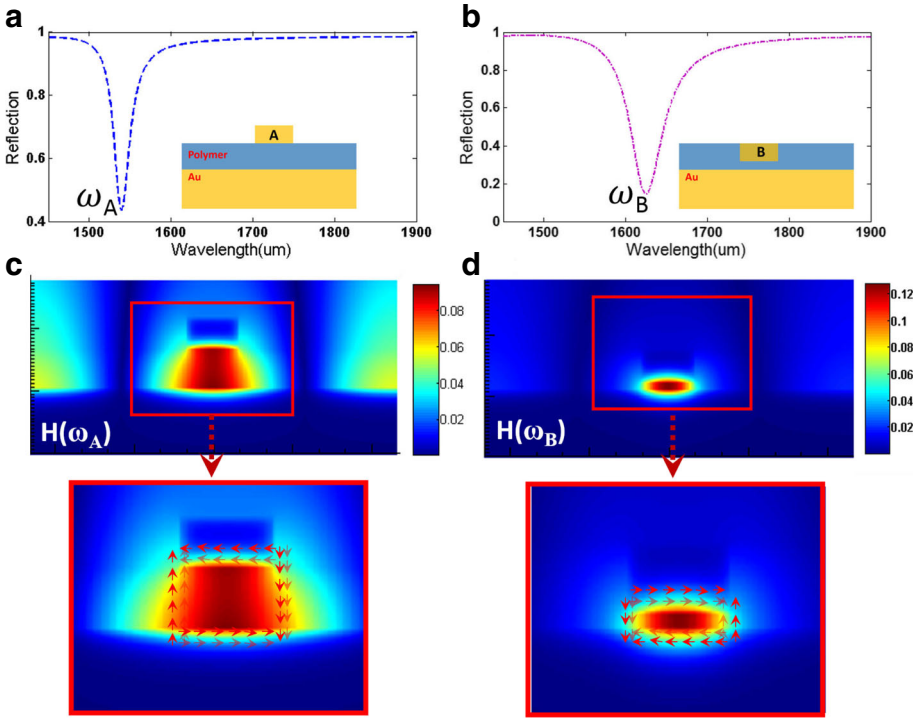

Fig. 4 a Reflection spectrum of the plasmonic metasurface with only the gold nanobar A. **b** Reflection spectrum of the plasmonic metasurface with only the gold nanobar B. **c** Calculated magnetic field distributions H of the metasurface at resonant wavelengths of ω_A mode. **d** Calculated magnetic field distributions H of the metasurface at resonant wavelengths of ω_B mode. (The thickness of both gold A and gold B is 92 nm; the width of both gold A and gold B is 92 nm; the thickness of polymer is 110 nm; the period is 1395 nm)

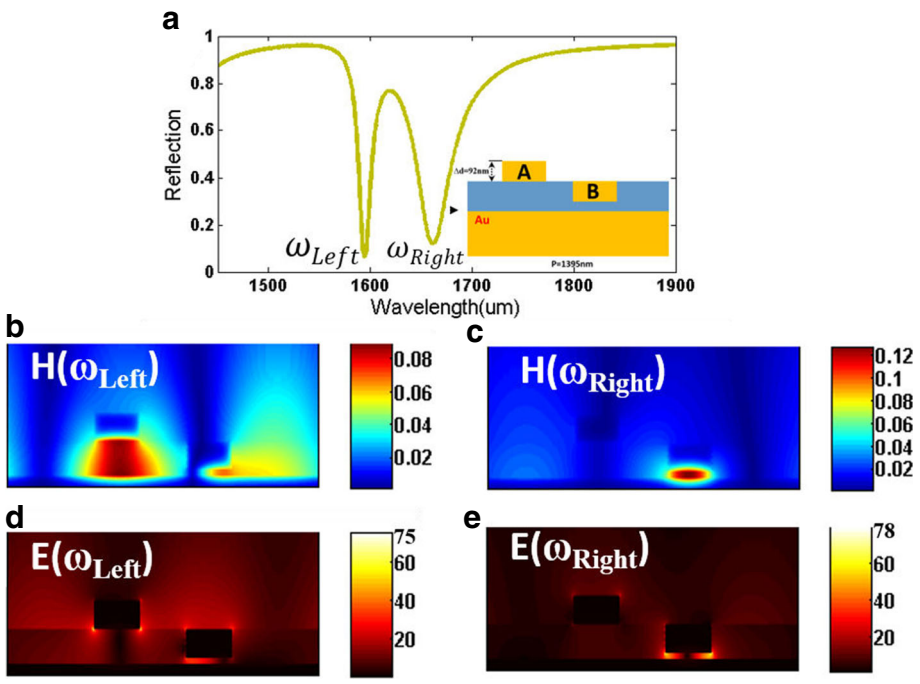

Fig. 5 a Reflection spectrum of the plasmonic metasurface shown in Fig. 2. **b**, **c** Calculated magnetic field distributions H of the metasurface at resonant wavelengths of the ω_{Left} mode and ω_{Right} mode, respectively. **d**, **e** Calculated electric field distributions ($|E_{loc}|/|E_0|$) of the metasurface at resonant wavelengths of the ω_{Left} mode andω_{Right} mode, respectively

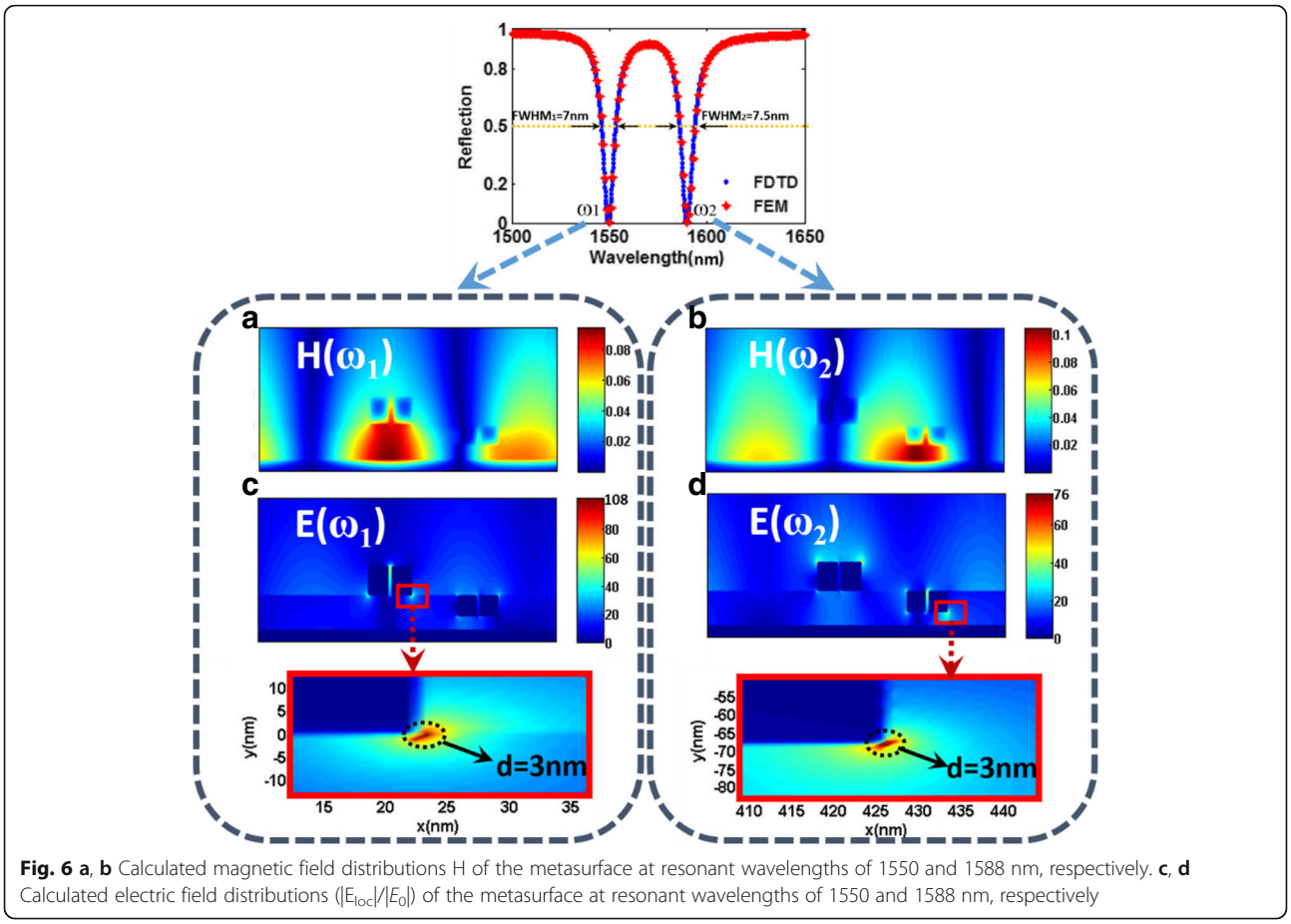

Fig. 6 **a**, **b** Calculated magnetic field distributions H of the metasurface at resonant wavelengths of 1550 and 1588 nm, respectively. **c**, **d** Calculated electric field distributions ($|E_{loc}|/|E_0|$) of the metasurface at resonant wavelengths of 1550 and 1588 nm, respectively

is mainly located in the gap between the gold bar and the gold substrate, and part of magnetic field is propagated to the nanosilt between two gold nanobars. Different from the electric field only resulting from the out-of-plane coupling as shown in Fig. 5d, e, the electric field of this proposed metasurface is also strongly localized within an ultrasmall area between the two gold bars according to Fig. 6c, d, which signifies the strong localized surface plasmon (LSP) coupling between the two gold nanobars. Figure 6c shows that the maximum electric field enhancement at the resonant wavelength can reach as high as 108, around 1.4 times compared to the only film-coupled metasurface shown in Fig. 5d, which is much higher than those of the previously reported nanoantennas [21, 60–65]. Particularly, we can clearly observe that the ultrasmall "hot spot" featured by the strong electric enhancement is confined within a circular area with a diameter of only 3 nm. Thus, these hybridized metasurface systems have been shown to simultaneously have superior absorption, large local electric enhancement, and small lateral resolution, which are very helpful for probing the accurate properties of single molecules for many surface-enhanced spectroscopies, due to their ability of supporting both the LSP and out-of-plane couplings.

From the analysis results in Fig. 2b, we know that the metasurface couples efficiently for TM polarization and remains dark for TE polarization, owing to asymmetric design, which has a potential application in polarization switch. Then, considering that the refractive index of PVA (poly(vinyl alcohol) can be changed with alteration of pump power [36, 56, 57], the operating wavelength of plasmonic resonances generally can be changed by varying the refractive index of dielectric layer. Then, Fig. 7a,b illustrates that the proposed metasurface can indeed work as a polarization switch, which is based on a reflective polarizer containing a tunable resonance for TM-polarized light by changing the refractive index of PVA. Clearly, as shown in Fig. 7b, without an external stimulus, the TM-polarized light is completely absorbed at wavelength of 1550 nm ("off" state), and this metasurface can completely reflect the TM-polarized light at wavelength of 1565 nm ("on" state). With an external stimulus, the Fano resonance for the TM-polarized wave is shifted to 1565 nm ("off" state), and this metasurface becomes completely reflective for TM-polarized light at 1550 nm ("on" state). Clearly, in Fig. 7b, this metasurface can realize a reflection value change from 0.009 to 98% at 1550 nm, and such a large modulation depth is far

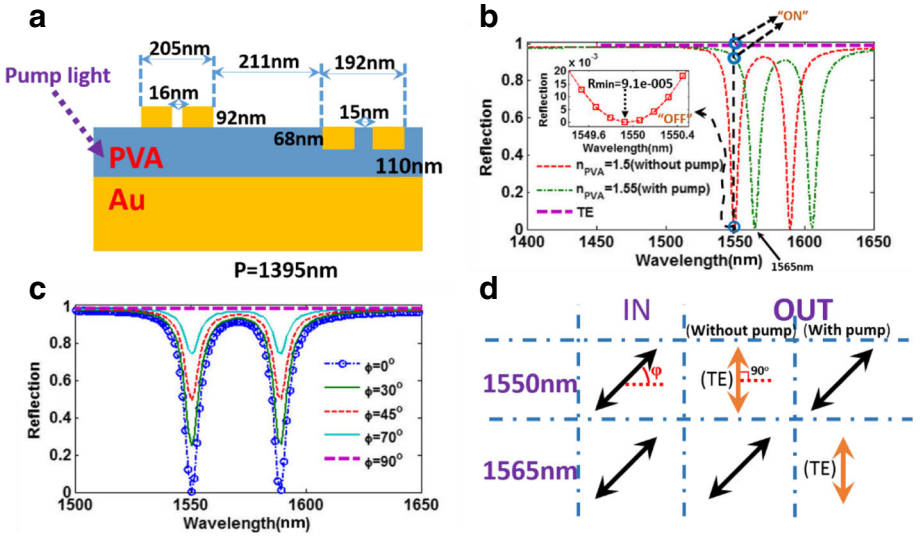

Fig. 7 **a** Schematic structure of the proposed metasurface with pump light. **b** The reflection spectra of the proposed metasurface with TM- and TE-polarized incident light, with and without pump light. **c** The reflection spectra of the proposed metasurface with various polarization angles. **d** The projected output polarizations of the metasurface, with and without a pump, at 1550 and 1588 nm

higher than previously reported plasmonic switch systems. On the other hand, according to Fig. 7b, the reflection of the incident light remains close to one with and without the external stimulus for TE polarization ("on" state). Therefore, this metasurface can realize a polarization switch for TM-polarized light based on a reflective polarizer with an extinction ratio of 11,000 (R_{TE}/R_{TM} = 0.99/0.00009 = 11,000) at 1550 nm. We also give a calculation about the effect of polarization angle ϕ on the reflection spectra, as shown in Fig. 7c. Clearly, the absorption performance will gradually deteriorate at the resonant wavelengths with increasing ϕ, which can be explained by that the incident electric field E can be decomposed into TE- and TM-polarized light and the TE-polarized light is reflected. Based on the calculated results in Fig. 7c, the projected output polarizations of the metasurface, with and without a pump, at 1550 and 1588 nm are plotted in Fig. 7d.

In-doped CdO is one kind of optically tunable plasmonic material, and the femtosecond polarization switch operating at 2.8 μm based on the photoexcited CdO film has been demonstrated experimentally in the recent literature [1]. In order to further improve the tunable capacity of our EIT structure, we investigate the optical properties of the proposed metasurface using CdO [1]. The schematic structure of the CdO-based metasurface with geometric parameters is depicted in Fig. 8a. The refractive index of MgO and CdO is obtained from references [1, 66], respectively. According to Fig. 8b, we show the reflection spectra with and without a pump around 1568 nm. In the static "on" state, the proposed metasurface is a polarizer that reflects the TE-polarized wave and completely absorbs the TM-polarized wave at wavelength 1568 nm. In the static "off" state, the proposed metasurface becomes reflective for both TM and TE polarizations at 1568 nm, and the resonance for TM-polarized wave is shifted to 1581 nm, owing to the

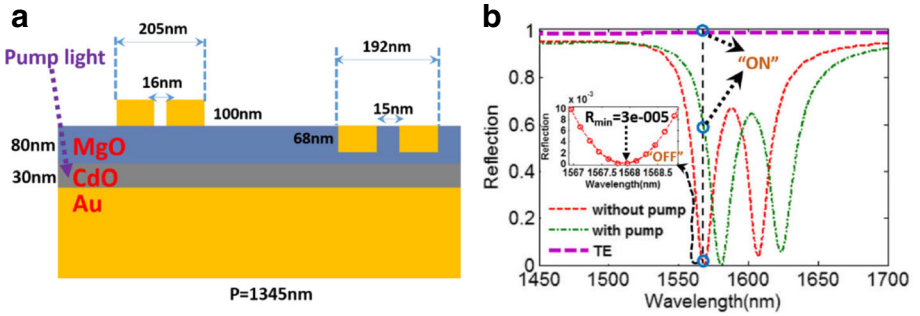

Fig. 8 **a** Schematic structure of the CdO-based metasurface with pump light. **b** The reflection spectra of the CdO-based metasurface with TM- and TE-polarized incident light, with and without pump light

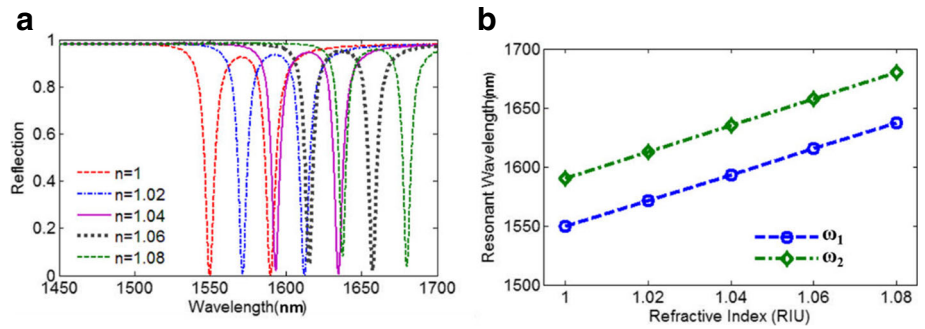

Fig. 9 **a** Reflection spectra of the proposed metasurface with varying refractive index of surrounding environment. **b** Resonant wavelengths of the proposed metasurface as a function of the surrounding refractive index

refractive index change of In-doped CdO by an external stimulus. Particularly, this reflective polarizer can achieve a huge extinction ratio at 1568 nm for TM-polarized light owing to the extremely low R_{min} shown in Fig. 8b. The huge extinction ratio of the CdO-based metasurface make it a good platform for active polarization control. Note that, the refractive index of the CdO can be tuned by changing pump power, which also can realize active control of the operating wavelength of the EIT-like effect. Besides, we can find that the pump light has no influence to the other materials (including gold, MgO), which have been demonstrated by experiments in these references [1, 36, 56, 57].

Besides, for the sensitivity of refractive index from the above analysis, the proposed metasurface also can be applied to detect the change of refractive index of surrounding environment. In many previously reported works about refractive index sensing, the light intensity of reflection/transmission wave is usually measured when the surrounding refractive index is variable with a specific operating wavelength. Then, to demonstrate the sensing property of this metasurface, Fig. 9 presents that the double plasmonic resonances are red-shifted with the increasing of surrounding refractive index changes. With the variation of the surrounding refractive index, the sensitivity(S) can reach S = 1500 nm/RIU. Then, the FWHM of the reflection dip at ω_1 and ω_2 is 7 and 7.5 nm respectively, which indicate that this metasurface can operate as an ultra-high FOM($S/FWHM_1 = 214.29$) refractive index sensor in the near infrared region. The FOM = 214.29 is much higher than those of most previously reported plasmonic refractive index sensor [58, 67–70].

Conclusions

In this work, a novel optically tunable hybridized metasurface is proposed and exploited to generate the EIT-like phenomena around 1550 nm, which hybridizes the in-plane near-field coupling between gold nanobars and the out-of-plane near-field between gold nanobars and substrate. For the traditional design of EIT-like metamaterials, two different shaped resonators, in planar or vertical arrangement, are working as bright mode and dark mode respectively, which can induce EIT effect by bright-dark mode coupling. However, in this structure, the two individual bright modes mainly result from the two same shaped resonators with different positions, which is neither a planar structure nor a vertical structure. The resulting two fundamental plasmon modes of the hybridized system are also investigated in detail. By introducing indium-doped CdO, the operating wavelength of the EIT-like phenomenon can be tuned optically. At the same time, this metasurface is firstly demonstrated to be a femtosecond polarization switch for TM-polarized light at 1550 nm, which can realize an extinction ratio (R_{TE}/R_{TM}) much higher than that of previously reported polarization switches. Besides, operating as plasmonic nanoantennas, this metasurface also achieves a strong local field enhancement ($|E_{loc}|/|E_0| > 100$) and a near-perfect absorption (> 99%) simultaneously. Owing to these above advantages, this proposed metasurface is a promising candidate for femtosecond polarization switching, plasmonic nanoantennas, and high FOM refractive index sensor.

Abbreviations

EIT: Electromagnetically induced transparency; FDTD: Finite difference time domain; FE: Field enhancement; FEM: Finite element method; FOM: Figure of merit; FWHM: Full width at half maximum; PML: Perfectly matched layer; SEIRA: Surface-enhanced infrared absorption; SERS: Surface-enhanced Raman scattering

Funding

National Key R&D Program of China (2016YFA0301300); National Natural Science Foundation of China (NSFC)(61275201, 61372037); Beijing Excellent Ph.D. Thesis Guidance Foundation (20131001301); BUPT Excellent Ph.D. Students Foundation (CX2017401).

Availability of Data and Materials

The datasets generated during and/or analyzed during the current study are available from the corresponding authors on reasonable request.

Authors' Contributions

DW, LY, and CL carried out the simulation and analysis. ZX, YL, ZY, and LY wrote the paper. LY, LC, and RM created the figures. HY supervised the whole work. DW and LY made the modification of the revised manuscript. All the authors reviewed the manuscript. All authors read and approved the final manuscript.

Competing Interests

The authors declare that they have no competing interests.

Publisher's Note

Author details
[1]State Key Laboratory of Information Photonics and Optical Communications, Beijing University of Posts and Telecommunications, Beijing 100876, China. [2]School of Science, Beijing University of Posts and Telecommunications, Beijing 100876, China.

Received: 25 January 2018 Accepted: 30 April 2018
Published online: 10 May 2018

References

1. Yang YM, Kelley K, Sachet E, Campione S, Luk TS, Maria JP, Michael BS, Brener I (2017) Femtosecond optical polarization switching using a cadmium oxide-based perfect absorber. Nat Photonics 11:390
2. Zhang L, Mei ST, Huang K, Qiu CW (2016) Advances in full control of electromagnetic waves with metasurfaces. Adv Opt Mater 4:818–833
3. Liu ZH, Ye J (2016) Highly controllable double Fano resonances in plasmonic metasurfaces. Nano 8:17665–17674
4. Chen L, Xu NN, Singh L, Cui TJ, Singh R, Zhu YM, Zhang WL (2017) Defect-induced Fano resonances in corrugated plasmonic metamaterials. Adv Opt Mater 5:8
5. Dayal G, Chin XY, Soci C, Singh R (2016) High-Q whispering-gallery-mode-based plasmonic Fano resonances in coupled metallic metasurfaces at near infrared frequencies. Adv Opt Mater 4:1295–1301
6. Luk'yanchuk B, Zheludev NI, Maier SA, Halas NJ, Nordlander P, Giessen H, Chong CT (2010) The Fano resonance in plasmonic nanostructures and metamaterials. Nat Mater 9:707–715
7. Miroshnichenko AE, Flach S, Kivshar YS (2010) Fano resonances in nanoscale structures. Rev Mod Phys 82:2257–2298
8. Li Y, Li DZ, Chi C, Huang BL (2017) Achieving strong field enhancement and light absorption simultaneously with plasmonic nanoantennas exploiting film-coupled triangular nanodisks. J Phys Chem C 121:16481–16490
9. Lin LH, Zheng YB (2015) Optimizing plasmonic nanoantennas via coordinated multiple coupling. Sci Rep 5:14788
10. Bharadwaj P, Deutsch B, Novotny L (2009) Optical antennas. Adv Opt Photon 1:438–483
11. Kante B, Burokur SN, Sellier A, Lustrac A, Lourtioz JM (2009) Controlling plasmon hybridization for negative refraction metamaterials. Phys Rev B 79:7
12. Wu D, Liu Y, Chen L, Ma R, Liu C, Xiang C, Li R, Ye H (2017) Broadband mid-infrared dual-band double-negative metamaterial: realized using a simple geometry, plasmonics, pp 1–9 1-9
13. Zhu H, Yi F, Cubukcu E (2016) Plasmonic metamaterial absorber for broadband manipulation of mechanical resonances. Nat Photonics 1011: 709–714
14. Wu D, Liu Y, Xu Z, Yu Z, Yu L, Chen L, Liu C, Li R, Ma R, Zhang J, Ye H (2017) Numerical study of the wide-angle polarization-independent ultra-broadband efficient selective solar absorber in the entire solar spectrum. Solar RRL 1:1700049
15. Wu D, Liu C, Xu Z, Liu Y, Yu Z, Yu L, Chen L, Li R, Ma R, Ye H (2018) The design of ultra-broadband selective near-perfect absorber based on photonic structures to achieve near-ideal daytime radiative cooling. Mater Des 139:104–111
16. Chen K, Adato R, Altug H (2012) Dual-band perfect absorber for multispectral plasmon-enhanced infrared spectroscopy. ACS Nano 6:7998–8006
17. Amin M, Farhat M, Bagci H (2013) A dynamically reconfigurable Fano metamaterial through graphene tuning for switching and sensing applications. Sci Rep 3:2105
18. Aksyuk V, Lahiri B, Holland G, Centrone A (2015) Near-field asymmetries in plasmonic resonators. Nano 78:3634–3644
19. Yahiaoui R, Manjappa M, Srivastava YK, Singh R (2017) Active control and switching of broadband electromagnetically induced transparency in symmetric metadevices. Appl Phys Lett 111:1103–2109
20. Yang YM, Kravchenko II, Briggs DP, Valentine J (2014) All-dielectric metasurface analogue of electromagnetically induced transparency. Nat Commun 5:5753
21. Wu D, Liu YM, Yu L, Yu ZY, Chen L, Li RF, Liu C, Zhang J, Ye H (2017) Plasmonic metamaterial for electromagnetically induced transparency analogue and ultra-high figure of merit sensor. Sci Rep 7:45210
22. Zhang S, Genov DA, Wang Y, Liu M, Zhang X (2008) Plasmon-induced transparency in metamaterials. Phys Rev Lett 101:047401
23. Liu N, Langguth L, Weiss T, Kastel J, Fleischhauer M, Pfau T, Giessen H (2009) Plasmonic analogue of electromagnetically induced transparency at the Drude damping limit. Nat Mater 8:758–762
24. Zhang XQ, Xu Q, Li Q, Xu YH, Gu JQ, Tian Z, Ouyang C, Liu Y, Zhang S, Zhang X, Han J, Zhang W (2016) Asymmetric excitation of surface plasmons by dark mode coupling. Sci Adv 2:e1501142–e1501142
25. Xie JY, Zhu X, Zang XF, Cheng QQ, Ye YY, Zhu YM (2017) High extinction ratio electromagnetically induced transparency analogue based on the radiation suppression of dark modes. Sci Rep 7:11291
26. Li HM, Liu SB, Liu SY, Wang SY, Ding GW, Yang H, Yu ZF, Zhang HF (2015) Low-loss metamaterial electromagnetically induced transparency based on electric toroidal dipolar response. Appl Phys Lett 106:1107
27. Jung H, In C, Choi H, Lee H (2016) Electromagnetically induced transparency analogue by self-complementary terahertz meta-atom. Adv Opt Mater 4:627–633
28. Monticone F, Alu A (2017) Metamaterial, plasmonic and nanophotonic devices reports on progress in physics, vol 80
29. Mun SE, Lee K, Yun H, Lee B (2016) Polarization-independent Plasmon-induced transparency in a symmetric metamaterial. IEEE Photon Technol Lett 28:2581–2584
30. Naik GV, Shalaev VM, Boltasseva A (2013) Alternative Plasmonic materials: beyond gold and silver. Adv Mater 25:3264–3294
31. Wang JQ, Yuan BH, Fan CZ, He JN, Ding P, Xue QZ, Liang EJ (2013) A novel planar metamaterial design for electromagnetically induced transparency and slow light. Opt Express 21:25159–25166
32. Zhao XL, Yuan C, Zhu L, Yao JQ (2016) Graphene-based tunable terahertz plasmon-induced transparency metamaterial. Nano 8:15273–15280
33. Zhu L, Meng FY, Dong L, Fu JH, Zhang F, Wu Q (2013) Polarization manipulation based on electromagnetically induced transparency-like EIT-like effect. Opt Express 21:32099–32110
34. Zhu L, Meng FY, Fu JH, Wu Q (2012) An electromagnetically induced transparency metamaterial with polarization insensitivity based on multi-quasi-dark modes. J Phys D-Appl Phys 45:445105–445105
35. Pitchappa P, Manjappa M, Ho CP, Singh R, Singh N, Lee C (2016) Active control of electromagnetically induced transparency analog in terahertz MEMS metamaterial. Adv Opt Mater 4:541–547
36. Chen JJ, Li Z, Yue S, Gong QH (2011) Highly efficient all-optical control of surface-plasmon-polariton generation based on a compact asymmetric single slit. Nano Lett 11:2933–2937
37. Cong JW, Yao HB, Gong DL, Chen MY, Tong YQ, Fu YH, Ren NF (2016) Broadening of absorption band by coupled gap plasmon resonances in a near-infrared metamaterial absorber. Appl Phys Express 9:072001
38. Han S, Cong LQ, Gao F, Singh R, Yang HL (2016) Observation of Fano resonance and classical analog of electromagnetically induced transparency in toroidal metamaterials. Ann Phys 528:352–357
39. Shaltout AM, Kinsey N, Kim J, Chandrasekar R, Ndukaife JC, Boltasseva A, Shalaev VM (2016) Development of optical metasurfaces: emerging concepts and new materials. Proc IEEE 104:2270–2287
40. Zhang YD, Li H, Wu YF, Zhang XN (2015) Fano resonances in nanoscale plasmonic structure, plasmonics: metallic nanostructures and their optical properties xiii, vol 9547
41. Hokari R, Kanamori Y, Hane K (2014) Comparison of electromagnetically induced transparency between silver, gold, and aluminum metamaterials at visible wavelengths. Opt Express 22:3526–3537
42. Liu HL, Leong ESP, Wang ZL, Si GY, Zheng LJ, Liu YJ, Soci C (2013) Multiple and multipolar Fano resonances in plasmonic nanoring pentamers. Adv Opt Mater 1:978–983
43. Miyamaru F, Morita H, Nishiyama Y, Nishida T, Nakanishi T, Kitano M, Takeda MW (2014) Ultrafast optical control of group delay of narrow- band terahertz waves. Sci Rep 4:4346
44. Xia SX, Zhai X, Wang LL, Sun B, Liu JQ, Wen SC (2016) Dynamically tunable plasmonically induced transparency in sinusoidally curved and planar graphene layers. Opt Express 24(16):17886–17899
45. Bull JD, Jaeger NAF, Kato H, Fairburn M, Reid A, Ghanipour P (2004) 40-GHz electro-optic polarization modulator for fiber optic communications systems. Proc SPIE 5577:133–143
46. Eklund H, Roos A, Eng ST (1975) Rotation of laser beam polarization in acoustooptic devices. Opt Quant Electron 7:73–79
47. MacDonald KF, Sámson ZL, Stockman MI, Zheludev NI (2009) Ultrafast active plasmonics. Nat Photon 3:55–58

48. Xia SX, Zhai X, Huang Y, Liu JQ, Wang LL, Wen SC (2017) Graphene surface plasmons with dielectric metasurfaces. J Lightwave Technol 35(20):4553–4558
49. Xia SX, Zhai X, Huang Y, Liu JQ, Wang LL, Wen SC (2017) Multi-band perfect plasmonic absorptions using rectangular graphene gratings. Opt Lett 42(15): 3052–3055
50. Guo PJ, Schaller RD, Ketterson JB, Chang RPH (2016) Ultrafast switching of tunable infrared plasmons in indium tin oxide nanorod arrays with large absolute amplitude. Nat Photonics 10:267
51. Sim S, Jang H, Koirala N, Brahlek M, Moon J, Sung JH, Park J, Cha S, Oh S, Jo MH, Ahn JH, Choi H (2015) Ultra-high modulation depth exceeding 2,400% in optically controlled topological surface plasmons. Nat Commun 6:8814
52. Tyborski T, Kalusniak S, Sadofev S, Henneberger F, Woerner M, Elsaesser T (2015) Ultrafast nonlinear response of bulk plasmons in highly doped ZnO layers. Phys Rev Lett 115:14
53. Wagner M, Fei Z, McLeod AS, Rodin AS, Bao WZ, Iwinski EG, Basov DN (2014) Ultrafast and nanoscale plasmonic phenomena in exfoliated graphene revealed by infrared pump-probe Nanoscopy. Nano Lett 14:894–900
54. Wagner M, McLeod AS, Maddox SJ, Fei Z, Liu MK, Averitt RD, Basov DN (2014) Ultrafast dynamics of surface plasmons in InAs by time-resolved infrared nanospectroscopy. Nano Lett 14:4529–4534
55. Wurtz GA, Pollard R, Hendren W, Wiederrecht GP, Gosztola DJ, Podolskiy VA, Zayats AV (2011) Designed ultrafast optical nonlinearity in a plasmonic nanorod metamaterial enhanced by nonlocality. Nat Nanotechnol 6:106–110
56. Chen JJ, Li Z, Yue S, Xiao JH, Gong QH (2012) Plasmon-induced transparency in asymmetric T-shape single slit. Nano Lett 12:2494–2498
57. Chen JJ, Li Z, Zhang X, Xiao JH, Gong QH (2013) Submicron bidirectional all-optical plasmonic switches. Sci Rep 3:1451
58. Luo SW, Zhao J, Zuo DL, Wang XB (2016) Perfect narrow band absorber for sensing applications. Opt Express 24:9288–9294
59. Wu D, Liu YM, Li RF, Chen L, Ma R, Liu C, Ye H (2016) Infrared perfect ultra-narrow band absorber as plasmonic sensor. Nanoscale Res Lett 11:483
60. Alaee R, Menzel C, Huebner U, Pshenay-Severin E, Bin Hasan S, Pertsch T, Rockstuhl C, Lederer F (2013) Deep-subwavelength plasmonic nanoresonators exploiting extreme coupling. Nano Lett 13:3482–3486
61. Seok TJ, Jamshidi A, Kim M, Dhuey S, Lakhani A, Choo H, Schuck PJ, Cabrini S, Schwartzberg AM, Bokor J (2011) Radiation engineering of optical antennas for maximum field enhancement. Nano Lett 11:2606–2610
62. Chu Y, Schonbrun E, Yang T, Crozier KB (2008) Experimental observation of narrow surface plasmon resonances in gold nanoparticle arrays. Appl Phys Lett 93:181108
63. Linden S, Niesler FBP, Förstner J, Grynko Y, Meier T, Wegener M (2012) Collective effects in second-harmonic generation from split-ring-resonator arrays. Phys Rev Lett 109:015502
64. Chu Y, Banaee MG, Crozier KB (2010) Double-resonance plasmon substrates for surface-enhanced Raman scattering with enhancement at excitation and stokes frequencies. ACS Nano 4:2804–2810
65. Lassiter JB, Chen X, Liu X, Ciracì C, Hoang TB, Larouche S, Oh SH, Mikkelsen MH, Smith DR (2014) Third-harmonic generation enhancement by film-coupled plasmonic stripe resonators. ACS Photonics 1:1212–1217
66. Stephens RE, Malitson IH (1952) Index of refraction of magnesium oxide. J Res Natl Bur Stand 49:249–252
67. Kuznetsov AI, Evlyukhin AB, Goncalves MR, Reinhardt C, Koroleva A, Arnedillo ML, Kiyan R, Marti O, Chichkov BN (2011) Laser fabrication of large-scale nanoparticle arrays for sensing applications. ACS Nano 5:4843–4849
68. Offermans P, Schaafsma MC, Rodriguez SRK, Zhang YC, Crego-Calama M, Brongersma SH, Rivas JG (2011) Universal scaling of the figure of merit of plasmonic sensors. ACS Nano 5:5151–5157
69. Shen Y, Zhou JH, Liu TR, Tao YT, Jiang RB, Liu MX, Xiao GH, Zhu JH, Zhou ZK, Wang XH, Jin CJ, Wang JF (2013) Plasmonic gold mushroom arrays with refractive index sensing figures of merit approaching the theoretical limit. Nat Commun 4:2381
70. Spackova BB, Homola J (2013) Sensing properties of lattice resonances of 2D metal nanoparticle arrays: an analytical model. Opt Express 21:27490–27502